Microfluidic breakups of confined droplets against a linear obstacle: The importance of the viscosity contrast.

Louis Salkin, Laurent Courbin, Pascal Panizza

Microfluidic breakups of confined droplets against a linear obstacle: The importance of the viscosity contrast

Louis Salkin, Laurent Courbin,* and Pascal Panizza†
IPR, UMR CNRS 6251, Campus Beaulieu, Université Rennes 1, 35042 Rennes, France
(Received 15 September 2011; published 21 September 2012)

Combining experiments and theory, we investigate the break-up dynamics of deformable objects, such as drops and bubbles, against a linear micro-obstacle. Our experiments bring the role of the viscosity contrast $\Delta\eta$ between dispersed and continuous phases to light: the evolution of the critical capillary number to break a drop as a function of its size is either nonmonotonic ($\Delta\eta > 0$) or monotonic ($\Delta\eta \leqslant 0$). In the case of positive viscosity contrasts, experiments and modeling reveal the existence of an unexpected critical object size for which the critical capillary number for breakup is minimum. Using simple physical arguments, we derive a model that well describes observations, provides diagrams mapping the four hydrodynamic regimes identified experimentally, and demonstrates that the critical size originating from confinement solely depends on geometrical parameters of the obstacle.

DOI: 10.1103/PhysRevE.86.036317 PACS number(s): 47.55.df, 47.60.Dx, 47.61.Cb

I. INTRODUCTION

An everyday experience, the breaking of drops and bubbles, has been extensively studied in a variety of flow geometries [1,2] and in the physics, chemistry, and engineering of emulsions and foams [3,4]. Addressing this issue requires one to determine the minimum energy needed to break an object and the size and number of the created daughter objects. Recent advances in microfluidics, which offer possibilities for handling nanoliter fluid elements, have inspired investigations on the breakup of deformable objects in confined geometries [5–12]. Most of these studies on geometry-mediated breakups focus on droplets reaching T junctions [5–8], or junctions having arbitrary angles [9], while a few deal with flows past an obstacle, e.g., a square obstruction [5] or a circular post [12]. Microfluidic technologies raise challenging scientific questions and they are powerful tools for various applications that rely on the ability to perform and combine basic operations such as breaking deformable objects [13]. Yet, establishing a general theoretical framework that fully describes the break-up dynamics in confined geometries remains a challenging task because of the numerous governing parameters potentially at play: the size and speed of an object, the viscosities of dispersed and transporting phases, the surface tension, and the geometrical parameters.

Within this setting, here we discuss the breakup of confined drops in one particular geometry, namely, a linear obstacle. We show that the selected geometry allows for a solution to this complex problem: we identify the seven dimensionless quantities controlling the dynamics, and we present a theoretical framework that provides a full description of the break-up dynamics and accounts for the various experimental observations. Our model provides diagrams mapping the four hydrodynamic regimes identified experimentally. Our findings target the hidden nature of viscosity contrast between dispersed and transporting phases, as they reveal the unexpected existence of a critical drop size for which the critical capillary number for breakup is minimum in the case of positive viscosity contrasts.

II. EXPERIMENTS

A. Setup and materials

To study the physics of obstacle-mediated breakup, we work with planar microfluidic devices which consist of a drop generator based on a flow-focusing method [14], a dilution module [15] that enables control of the velocity of the drops without changing their size by infusing additional continuous phase, and a linear obstacle, placed in a rectangular microchannel of width $w = 130$ μm and height $h = 45$ μm [see Fig. 1(a)]. The devices are fabricated in polydimethylsiloxane (PDMS-Sylgard 184, Dow Corning) using standard soft lithography techniques [16]. The flow-focusing geometry produces periodic trains of monodisperse drops in an oil phase. We work with large drops, their size L_d is larger than w, herein referred to as "slugs." We use syringe pumps (PHD 2000, Harvard Apparatus) to inject the dispersed and continuous phases at controlled flow rates, which are adjusted independently until a steady flow of monodisperse slugs with a desired size $L_d = 150$–900 μm is obtained. Typical values of the corresponding flow rates for the dispersed and continuous phases are $q_w = 5-200$ μl/h and $q_o^f = 5-500$ μl/h, respectively. The dilution module enables control of the speed of the slugs $v = 0.1$–10 mm/s and the distance between slugs $\lambda = 600-2000$ μm by infusing additional continuous phase at a constant flow rate $q_o^d = 0-1000$ μl/h; hence the total flow rate is $q = q_w + q_o^f + q_o^d$. In all our experiments, the Reynolds and the capillary numbers are small and span the ranges $10^{-3}-10^{-1}$ and $10^{-3}-10^{-2}$, respectively. The linear obstacle of length $L = 200-800$ μm is parallel to the channel walls and is off-centered so that slugs may flow in two gaps (1) and (2), having different widths w_1 and $w_2 < w_1$, with $W = w_2/w_1 < 1$ [Fig. 1(a)]. In all our experiments, the interslug distance is large enough so that we study the breakups of isolated slugs. We record images of the flow close to the obstacle with a high-speed camera (Phantom V7) working at $500-5000$ frames/s. The speed and the size of a slug

*laurent.courbin@univ-rennes1.fr
†pascal.panizza@univ-rennes1.fr

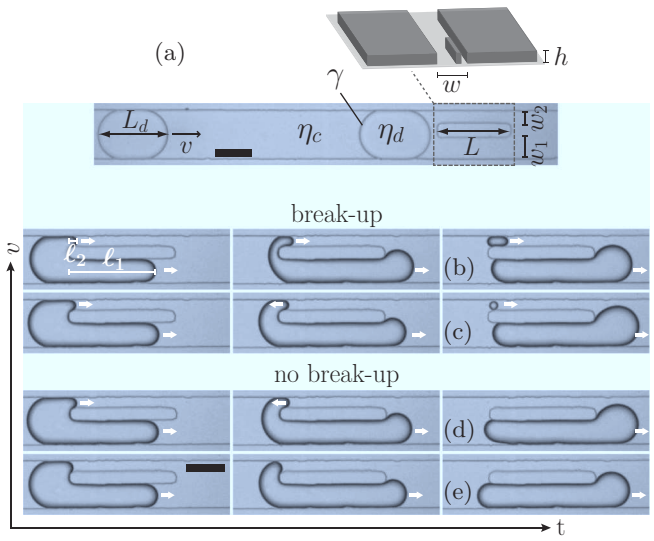

FIG. 1. (a) Schematic of the setup near the obstacle and top-view images of the flow defining the ten governing parameters at play. (b)–(e) Typical flow behaviors of slugs having the same size meeting an obstacle at different speeds. For large enough speeds, breakup occurs without (b) or with (c) the retraction of an interface in the narrow gap. The slug does not break at lower speeds; this occurs with the invasion and subsequent retraction of an interface of the narrow gap (d) or without the invasion of this gap (e). ℓ_i denotes the position of an interface in the ith gap, $i = 1$ or 2. White arrows indicate the flow direction in both gaps. Scale bars 100 μm.

are obtained from image processing using a custom-written MATLAB software.

We use two liquid-liquid systems. For the first one, we use different mass percentages of water-glucose mixtures (from 100/0 to 56/44) to vary the viscosity of the dispersed phase from $\eta_d = 1$–7 mPa s. The continuous phase is hexadecane (Sigma-Aldrich), whose viscosity is $\eta_c = 3$ mPa s. The interfacial tension between the two phases is $\gamma = 6.5$–5 mN/m, for the range of viscosities of the mixtures we prepare. The glucose is purchased from Sigma-Aldrich, and we use deionized water (Millipore, 18 MΩ cm). The second system consists of deionized water dispersed in a viscous silicone oil (Fluka) whose viscosity is $\eta_c = 50$ mPa s. The liquid-liquid surface tension is $\gamma = 9.7$ mN/m. For both systems, a surfactant (sodium dodecyl sulfate, Sigma) is solubilized in the dispersed phase (concentration, 15 g/L). Viscosities and surface tensions are measured using an Anton Paar MCR 301 rheometer and pendant drop tensiometry, respectively.

B. Experimental results

We begin by studying the response of a fluid system for which $\eta_d > \eta_c$. We vary v and we observe the behavior of slugs having the same size meeting the same linear obstacle. We find four different hydrodynamic regimes as v decreases [Figs. 1(b)–1(e) and movies S1–S4 in [17]). In the first two, the collision with the obstacle yields breakup. In the first, when a slug collides with the obstacle, two fluid-fluid interfaces invade gaps (1) and (2) and move forward. The slug breaks into two daughter drops emitted in both gaps when its rear edge meets the obstacle [Fig. 1(b) and movie S1] [17]. In the second, breakup is preceded by a drastically different dynamics of the two-fluid interface invading the narrow gap (2): as time elapses, it suddenly stops and begins to recede [Fig. 1(c) and movie S2]. In the third, a receding interface is also observed in the narrow gap; however, the slug does not break as its rear edge reaches the obstacle after total withdrawal of this interface [Fig. 1(d) and movie S3]. No propagation, and thus no retraction, is observed in gap (2) for lower speeds: the slug does not break and flows through gap (1) [Fig. 1(e) and movie S4] [17].

Systematic variations of v and L_d provide diagrams mapping these dynamical behaviors reported for two illustrative fluid systems whose viscosity contrasts have opposite signs [Figs. 2(a) and 2(b)]. When $\eta_d > \eta_c$, we observe two distinct sequences of regimes as v decreases for slugs either larger or smaller than a critical slug size L_d^{cr}. When $L_d > L_d^{cr}$,

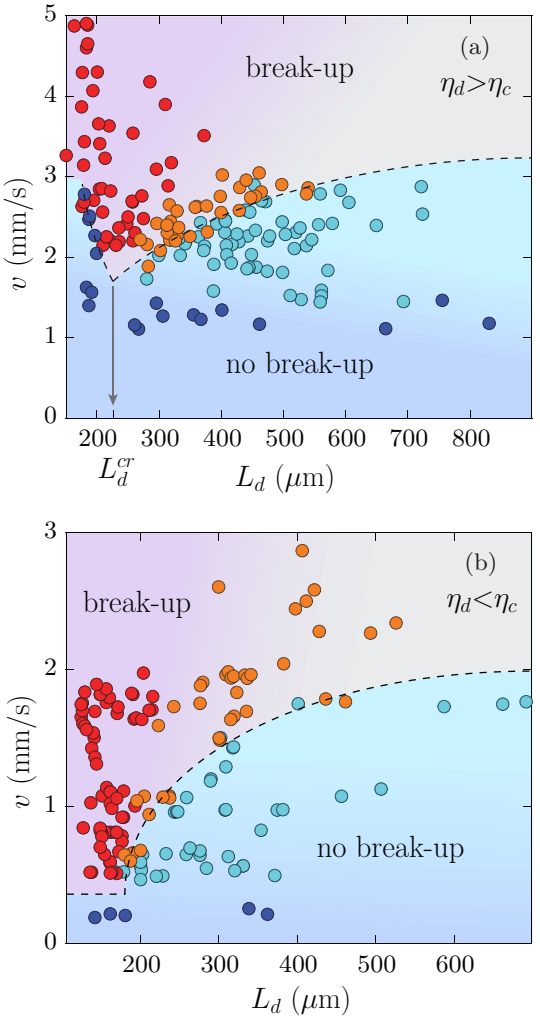

FIG. 2. (Color online) Experimental diagrams characterizing the dynamical behavior for (a) $\eta_d > \eta_c$ and (b) $\eta_d < \eta_c$ as a function of L_d and v. A slug may (orange and red symbols) or may not (blue and cyan symbols) break against the obstacle. These regimes can occur with (orange and cyan symbols) or without the retraction of a two-fluid interface in gap (2) (red and blue symbols). The dashed lines are guides for the eyes and indicate the transition between breakup and no breakup regimes. The length of the obstacle is $L = 300$ μm. (a) Viscous water-glucose mixture (44 wt.% glucose) in hexadecane and $W = 0.5$. (b) Water in a viscous silicone oil and $W = 0.6$.

we find the sequence of four regimes previously discussed. By contrast, only regimes without retraction in gap (2) are observed when $L_d < L_d^{cr}$ [Fig. 2(a)]. Remarkably, the transition between breakup and no-breakup regimes is nonmonotonic, with a global minimum point at $L_d = L_d^{cr}$. In addition, the critical slug speed to observe a two-fluid interface invading the narrow gap presents a crossover at $L_d \approx L_d^{cr}$, since this speed is constant for $L_d > L_d^{cr}$ and decreases with L_d for $L_d < L_d^{cr}$ [Fig. 2(a)]. By contrast, when $\eta_d < \eta_c$, the transition between breakup and no-breakup regimes is a monotonically increasing function of L_d, a critical slug size is not observed, and the critical speed at which an interface enters the narrow gap is constant over the whole range of slug sizes [Fig. 2(b)].

III. INTERPRETATION

A. Model

To explain the diversity of our findings, we begin by describing the transport of slugs in microfluidic conducts at low Reynolds and capillary numbers. Building on earlier works [12,18], we assume that the speed v of a slug flowing in a channel of constant cross section hw varies with q the total flow rate as $v = \frac{q}{hw}$, and that the flows of the slug and the continuous phase satisfy Darcy's law, with an effective viscosity η_d^{eff} for the slug [19]. Hence, the pressure drop Δp over a portion ℓ of the slug reads

$$\Delta p = \frac{\eta_d^{eff}\ell q}{h^3 w} f\left(\frac{w}{h}\right), \tag{1a}$$

where $f(\frac{w}{h})$ is a known dimensionless function which can be written $f \approx 12[1–0.63(\frac{w}{h})^{-1}]^{-1}$ for $h < w$ [20]. There is also a pressure drop across the front edge of the slug due to the curved two-fluid interface, which we write approximately as [9,12]

$$\Delta p_{curv} = \frac{2\gamma}{w}\left(1 + \frac{w}{h}\right). \tag{1b}$$

In our model, the pressure drop given in Eq. (1b) accounts for the presence of curved interfaces. However, for simplicity's sake, we derive our model considering flat interfaces rather than curved. These physical arguments help to rationalize the dynamics starting at $t = 0$ when a slug meets the obstacle. Since we work at constant flow rates, a two-fluid interface always invades gap (1) at $t = 0$ and begins to move forward at a speed $d\ell_1/dt$ [see Fig. 1(b) defining ℓ_1]. After the collision, our observations show that the velocity of the slug v remains roughly constant until the rear edge of the slug reaches the obstacle. In our simple model, since we consider slugs having flat interfaces, we assume that the time t_f at which the rear edge of the slug meets the obstacle is $t_f = \frac{L_d - cw}{v}$, where c is a free parameter $O(1)$ that depends on the dimensionless parameters of the cross section of the channel, i.e., $\frac{w}{h}$, $\frac{w_2}{h}$, and $\frac{w_2}{Wh}$. As breakup occurs, provided that a two-fluid interface has invaded gap (2) and has not completely withdrawn from this gap at t_f, we next work with the dimensionless time $T = \frac{t}{t_f}$.

B. Invasion of the narrow gap

We now derive the condition required to observe a two-fluid interface invading gap (2). We begin with the situation where one interface has entered the gap (1) and is located at $\ell_1(T) = X_1(T)L \leqslant L$. At T, the conservation of the total flow rate gives $X_1(T) = \frac{(L_d - cw)w}{Lw_1}T = \alpha T$ and, using Eq. (1), we write the pressure drop over L in gap (1), $\Delta p = \frac{\eta_c L q}{h^3 w_1} f_1[(1 + \Delta\eta X_1) + \frac{2Z}{\mathcal{C}}(1 + \frac{w_1}{h})]$, where $\Delta\eta = (\eta_d^{eff} - \eta_c)/\eta_c$ and $Z = (f_1 h^{-2} w L)^{-1}$ with $f_1 = f(\frac{w_1}{h})$ are two dimensionless parameters, and $\mathcal{C} = \frac{\eta_c v}{\gamma}$ is the capillary number. $\Delta\eta$ is a free parameter that depends on the unknown effective viscosity η_d^{eff}. The evolution of Δp over time strongly depends on the sign of $\Delta\eta$. When a low-viscosity fluid is displacing at constant flow rate a fluid having a larger viscosity, the pressure drop in gap (1) decreases with time. By contrast, when $\Delta\eta > 0$, Δp increases with T. As shown below, this dependence on $\Delta\eta$ controls the invasion dynamics of the narrow gap. Physically, a two-fluid interface may begin to fill up gap (2) only when Δp overcomes the capillary pressure $\frac{2\gamma}{w_2}(1 + \frac{w_2}{h})$ required for a curved interface to exist in this narrow gap. This condition can be mathematically expressed as $1 + \Delta\eta X_1 > \frac{\mathcal{C}_\star}{\mathcal{C}}$, where $\mathcal{C}_\star = 2Z\frac{1-W}{W}$. When $\Delta\eta < 0$, the term on the left-hand side of the inequality, $1 + \Delta\eta X_1$, decreases with T, so that the time T_p at which an interface begins to propagate in gap (2) is $T_p = 0$ whenever $\mathcal{C} > \mathcal{C}_\star$. By contrast, when $\Delta\eta > 0$, this term increases with T so that $T_p = \frac{1}{\alpha\Delta\eta}(\frac{\mathcal{C}_\star}{\mathcal{C}} - 1) \geqslant 0$. Two conditions need to be fulfilled to allow propagation in gap (2), $X_1(T_p) \leqslant 1$, which corresponds to the situation considered, and $T_p < 1$. Indeed, physically, invasion can no longer occur when the rear end of a slug reaches the obstacle, which gives the condition $T_p < 1$. Using these conditions, one finds that this occurs when $\mathcal{C} > \frac{\mathcal{C}_\star}{1+\alpha\Delta\eta}$ for $\alpha \leqslant 1$ and when $\mathcal{C} > \frac{\mathcal{C}_\star}{1+\Delta\eta}$ for $\alpha \geqslant 1$. For both positive and negative viscosity contrasts, if those conditions are not fulfilled when the fluid-fluid interface exits gap (1), the pressure drop in this gap suddenly decreases and remains constant over time, $\Delta p = \frac{\eta_c L q}{h^3 w_1} f_1(1 + \Delta\eta)$. In that case, the pressure drop can no longer become larger that the capillary pressure needed to accommodate the presence of a curved interface in the narrow gap and the invasion of the narrow gap never occurs. Our experiments concur with these theoretical predictions [Figs. 3(a) and 3(b)].

C. Dynamics of the two-fluid interfaces

At $T \geqslant T_p$, the dynamics of the interfaces present in both gaps are governed by a set of two coupled first-order ordinary differential equations. The conservation of the total flow rate gives the first equation:

$$\frac{dX_1}{dT} + W\frac{dX_2}{dT} = \alpha. \tag{2a}$$

The second equation is given by the equality of pressure drops over both sides of the obstacle:

$$(1 + \Delta\eta X_1)\frac{dX_1}{dT} - FW(1 + \Delta\eta X_2)\frac{dX_2}{dT} = \alpha\frac{\mathcal{C}_\star}{\mathcal{C}} \tag{2b}$$

for $X_1 \leqslant 1$ and $X_2 \leqslant 1$;

$$(1 + \Delta\eta)\frac{dX_1}{dT} - FW(1 + \Delta\eta X_2)\frac{dX_2}{dT} = \alpha\frac{\mathcal{C}_\star}{\mathcal{C}}\frac{1 + \frac{w_2}{h}}{1 - W} \tag{2c}$$

for $X_1 > 1$ and $X_2 \leqslant 1$, with $F = f(\frac{w_2}{h})/[Wf(\frac{w_2}{Wh})]$.

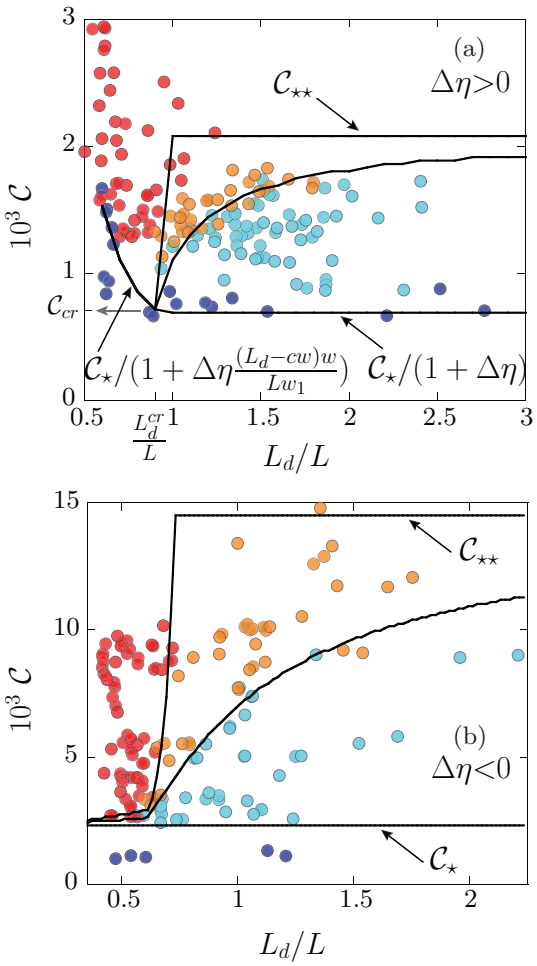

FIG. 3. (Color online) Diagrams mapping the break-up dynamics as a function of L_d/L and $\mathcal{C}$ for (a) $\Delta\eta > 0$ and (b) $\Delta\eta < 0$. The solid lines are predictions of our model for the transitions between regimes that are compared to experimental data of Figs. 2(a) and 2(b). Symbols are identical to those of Fig. 2. The dimensionless quantities are (a) $W = 0.5$, $\frac{w}{h} = 3$, $\frac{w_2}{h} = 0.7$, $Z = 2.4 \times 10^{-3}$, and (b) $W = 0.6$, $\frac{w}{h} = 3$, $\frac{w_2}{h} = 0.8$, $Z = 2.1 \times 10^{-3}$. The two free parameters are (a) $c = 0.9$ and $\Delta\eta = 8$, and (b) $c = 0.6$ and $\Delta\eta = -0.2$. The model predicts the critical capillary numbers above which an interface enters the gap (2): $\frac{\mathcal{C}_\star}{1+\Delta\eta}$ for $\Delta\eta > 0$ and $\alpha \geqslant 1$, $\frac{\mathcal{C}_\star}{1+\alpha\Delta\eta}$, for $\Delta\eta > 0$ and $\alpha \leqslant 1$, and $\mathcal{C}_\star$ for $\Delta\eta < 0$. When $\Delta\eta > 0$, we find that $\eta_d^{eff} > \eta_c$, which is consistent with the literature [21]. By contrast, when $\Delta\eta < 0$, we determine that $\eta_d < \eta_d^{eff} < \eta_c$. Similar results have been reported and discussed in [22].

D. Conditions for retraction

The retraction of a two-fluid interface in gap (2) observed in two regimes can be expressed as $\frac{dX_2}{dT} < 0$. Using Eq. (2), one finds that the sign of $\frac{dX_2}{dT}$ is given by the sign of $(1 + \Delta\eta X_1) - \frac{\mathcal{C}_\star}{\mathcal{C}}$ for $X_1 \leqslant 1$ and $X_2 \leqslant 1$, and by the sign of $(1 + \Delta\eta) - \frac{\mathcal{C}_\star}{\mathcal{C}}\frac{1+\frac{w_2}{h}}{1-W}$ for $X_1 > 1$ and $X_2 \leqslant 1$. Consequently, when $\Delta\eta \geqslant 0$, retraction may only begin when $X_1(T = T_1) = 1$, provided that $\mathcal{C} < \frac{\mathcal{C}_\star}{1+\Delta\eta}\frac{1+\frac{w_2}{h}}{1-W} = \mathcal{C}_{\star\star}$ and $T_1 < T_f = 1$; experimental observations corroborate this prediction (see movie S3 in [17]). By contrast, when $\Delta\eta < 0$, the retraction may occur at $T = T_r < T_1$, when the interface in gap (1) reaches the position $X_1(T_r) = \frac{1}{\Delta\eta}(\frac{\mathcal{C}_\star}{\mathcal{C}} - 1) < 1$, for $\mathcal{C} \leqslant \frac{\mathcal{C}_\star}{1+\Delta\eta}$ and $T_r < 1$. The retraction may also begin at $T = T_1$ when $\frac{\mathcal{C}_\star}{1+\Delta\eta} \leqslant \mathcal{C} < \mathcal{C}_{\star\star}$ and $T_1 < 1$. We use these conditions to compute numerically the transitions between the two break-up regimes. The resulting predictions concur with experiments [see Figs. 3(a) and 3(b)]. Analytical expressions for the transition between break-up regimes with and without retraction in gap (2) can also be derived both for $\Delta\eta > 0$ and $\Delta\eta < 0$ (see the Appendix); in both cases, the transition is a plateau given by $\mathcal{C} = \mathcal{C}_{\star\star}$ when L_d/L is large enough [see Figs. 3(a) and 3(b)].

E. Conditions for breakup

Breakup occurs whenever an interface has entered the narrow gap and $X_2(T = 1) > 0$. The transition between breakup and no-breakup regimes thus corresponds to $X_2(1) = 0$. Using this condition and solving Eq. (2), our numerical simulations well-capture this transition [Figs. 3(a) and 3(b)]. Interestingly, finding an analytical expression is straightforward when $\Delta\eta \geqslant 0$ and $\alpha \leqslant 1$: since $T_1 \geqslant 1$ for any value of $\mathcal{C}$, the retraction of an interface in gap (2) never occurs as observed experimentally [Fig. 3(a)]; breakup is obtained for $\mathcal{C} > \frac{\mathcal{C}_\star}{1+\alpha\Delta\eta}$. As suggested by the experiments, the model predicts a nonmonotonic and a monotonic transition for $\Delta\eta > 0$ and $\Delta\eta \leqslant 0$, respectively (Fig. 3). Our model therefore confirms the existence, when $\Delta\eta > 0$, of a characteristic size L_d^{cr} for which breaking occurs at a minimum capillary number $\mathcal{C}_{cr}$. Figure 4 shows that the experimental critical capillary number $\mathcal{C}_{cr}$ correlates with the predicted one $\mathcal{C}_\star/(1 + \Delta\eta)$. Studying the variations of L_d^{cr} for different fluid systems and values of Z, we find that the critical size does not depend on $\Delta\eta$ and varies with the geometrical parameters as the predicted

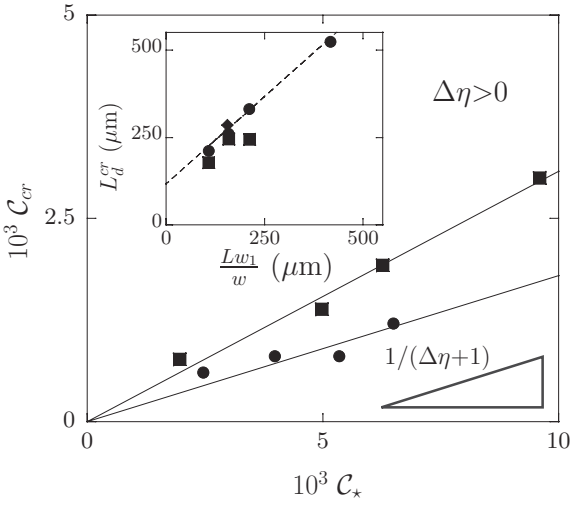

FIG. 4. Evolution of $\mathcal{C}_{cr}$ with $\mathcal{C}_\star$ for $\Delta\eta > 0$. For both fluid systems, the experimental data collapse onto a single line whose slope is $1/(\Delta\eta + 1)$. Inset: Evolution of the critical slug size L_d^{cr} with $\frac{Lw_1}{w}$. The fluid systems are (■) water in hexadecane, (♦) a viscous water-glucose (28 wt.% glucose) mixture in hexadecane, and (●) a viscous water-glucose mixture (44 wt.% glucose) in hexadecane. The ratio of the widths of the gaps is $W = 0.48$. Each data point corresponds to a value of $Z = 0.8$–3.8×10^{-3}. The dashed line stands for the linear fit $L_d^{cr} = \frac{Lw_1}{w} + 0.9w$.

expression $\frac{Lw_1}{w} + cw$ (inset of Fig. 4). In this figure, assuming that the value of c for $W = 0.48$ is close to the one ($c = 0.9$) determined for $W = 0.5$ in Fig. 3(a), we find that experiments correlate with theoretical predictions.

IV. CONCLUSION

Despite the apparent complexity of a problem with ten governing parameters [Fig. 1(a)], we provide a theoretical framework describing the break-up dynamics of deformable objects in terms of the pertinent dimensionless quantities $(\mathcal{C}, \frac{L_d}{L}, \Delta\eta, W, Z, \frac{w}{h}, \frac{w_2}{h})$. Our model is based on very strong approximations and its derivation employs the most basic physical arguments. Yet, for a given device, this model fully captures experimental observations in the plane $(\frac{L_d}{L}, \mathcal{C})$ using only two free parameters, the effective viscosity η_d^{eff} and the numerical constant c. Our findings bring the role of viscosity contrast to light, showing that the evolution of the critical capillary number to break a drop as a function of its size is either nonmonotonic ($\Delta\eta > 0$) or monotonic ($\Delta\eta \leqslant 0$). These results uncover a critical size originating from confinement for which the critical capillary number for breakup is minimum when the viscosity contrast is positive. The break-up dynamics of drops against a linear obstacle bear a resemblance to the well-known Saffman-Taylor instability [23], a problem which originates from the displacement of a fluid by another one and depends on the viscosity contrast between the two fluids [24]. In closing, it is worthwhile mentioning that similar experiments can be performed with bubbles rather than drops. As our model also predicts the volumes of both daughter drops or bubbles created upon breakup [25], this could help the design of commercial obstacle-mediated break-up devices for tailoring bidisperse emulsions and foams [26].

ACKNOWLEDGMENTS

We thank l'Université Européenne de Bretagne for partial support of this research (EPT *Physfood*). We thank A. Saint-Jalmes for helping us with the surface tension and viscosity measurements.

APPENDIX: ANALYTICAL DERIVATIONS OF THE TRANSITIONS BETWEEN BREAK-UP REGIMES WITH AND WITHOUT RETRACTION IN GAP (2)

1. *The case* $\Delta\eta > 0$

As explained in the main text, for $\Delta\eta \geqslant 0$, the withdrawal of the two-fluid interface in gap (2) occurs at $T = T_1$, provided that $\mathcal{C} < \frac{2Z}{1+\Delta\eta}\frac{1+\frac{w_2}{h}}{W} = \mathcal{C}_{\star\star}$ and $T_1 < 1$. One has to make a distinction between two possible cases, depending on whether $\alpha \geqslant 1$ or $\alpha \leqslant 1$. When $\alpha \geqslant 1$, by integrating Eq. (2a) between T_p and T_1, using $X_2(T_1) = \frac{\alpha T_1 - 1}{W}$, $X_2(T_p) = 0$, $X_1(T_1) = 1$, and the expression of T_p derived in the text, it is straightforward to show that T_1 is a solution of the following quadratic equation:

$$\frac{\Delta\eta F}{2W}\alpha^2 T_1^2 + \alpha T_1\left[\frac{\mathcal{C}_\star}{\mathcal{C}} + F\left(1 - \frac{\Delta\eta}{W}\right)\right] + \Delta\eta\frac{F-W}{2W} - (1+F) - \frac{\delta}{2\Delta\eta}\left(\frac{\mathcal{C}_\star}{\mathcal{C}} - 1\right)^2 = 0, \tag{A1}$$

where $\delta = 0$ for $\mathcal{C} \geqslant \mathcal{C}_\star$, and $\delta = 1$ for $\mathcal{C} \leqslant \mathcal{C}_\star$. Consequently, the condition $T_1 < 1$ imposes that $\mathcal{C} < \frac{\mathcal{C}_\star}{Y}$, where Y is the positive solution of the following equation:

$$\frac{\Delta\eta F}{2W}\alpha^2 + \left[\alpha F\left(1 - \frac{\Delta\eta}{W}\right) + \Delta\eta\frac{F-W}{2W} - (1+F)\right] + \alpha Y - \delta\frac{(Y-1)^2}{2\Delta\eta} = 0. \tag{A2}$$

In the $(\frac{L_d}{L}, \mathcal{C})$ plane, breakup without the retraction of the interface in gap (2) therefore occurs when $\mathcal{C}$ is larger than the critical capillary number $\min(\mathcal{C}_{\star\star}, \frac{\mathcal{C}_\star}{Y})$.

When $\alpha \leqslant 1$, as discussed in the main text, one finds a single transition between regimes without a receding interface in the narrow gap, breakup being observed when $\mathcal{C} > \frac{\mathcal{C}_\star}{1+\alpha\Delta\eta}$.

2. *The case* $\Delta\eta < 0$

The situation is slightly more complex when $\Delta\eta < 0$. As pointed out in the text, when $\mathcal{C} \leqslant \frac{\mathcal{C}_\star}{1+\Delta\eta}$, the retraction of the two-fluid interface in gap (2) may occur when $X_1 < 1$, at a time $T = T_r$ at which the fluid-fluid interface present in gap (1) reaches the position $X_1(T_r) = \frac{1}{\Delta\eta}(\frac{\mathcal{C}_\star}{\mathcal{C}} - 1)$. Following a similar approach to the one described above, integrating Eq. (2a) between $T = 0$ and T_r, and using $X_2(T_r) = \frac{\alpha T_r - X_1(T_r)}{W}$ and $X_2(0) = 0$, one shows that T_r is the solution of the following quadratic equation:

$$\frac{\Delta\eta F}{2W}\alpha^2 T_r^2 + \alpha T_r\left[\frac{\mathcal{C}_\star}{\mathcal{C}}\left(1 - \frac{F}{W}\right) + F\left(1 + \frac{1}{W}\right)\right] - \frac{1}{\Delta\eta}\left(\frac{\mathcal{C}_\star}{\mathcal{C}} - 1\right)\left[1 + F + \frac{1}{2W}\left(\frac{\mathcal{C}_\star}{\mathcal{C}} - 1\right)(W - F)\right] = 0. \tag{A3}$$

One experimentally witnesses such a phenomenon only provided that $T_r < 1$, a condition imposing that $\mathcal{C} < \frac{\mathcal{C}_\star}{Y}$, where Y is now the positive solution of the following second-degree polynomial equation:

$$\frac{\Delta\eta F}{2W}\alpha^2 + \alpha\left[Y\left(1 - \frac{F}{W}\right) + F\left(1 + \frac{1}{W}\right)\right] - \frac{Y-1}{\Delta\eta}\left[1 + F + \frac{Y-1}{2W}(W - F)\right] = 0. \tag{A4}$$

Although in the case $\mathcal{C} \geqslant \frac{\mathcal{C}_\star}{1+\Delta\eta}$ withdrawal of the two-fluid interface in gap (2) can no longer be observed for $X_1 < 1$, it may begin at $T_r = T_1$, when $X_1(T_1) = 1$, provided that $\mathcal{C} < \mathcal{C}_{\star\star}$. Since $T_p = 0$, following the same approach as the one used in Sec. I, one shows that T_1 is a solution of Eq. (A1) with $\delta = 0$. To observe receding, the condition $T_1 < 1$ must hold. This additional condition imposes that

$$\mathcal{C} < \frac{\alpha\mathcal{C}_\star}{1 + F - \frac{\Delta\eta}{2W}(F - W) - \frac{F\Delta\eta\alpha^2}{2W} - \alpha F\left(1 - \frac{\Delta\eta}{W}\right)}$$

To summarize, in the $(\frac{L_d}{L}, \mathcal{C})$ plane, breakup without a receding interface in gap (2) is observed when $\mathcal{C}$ is larger than the critical capillary number $\frac{\mathcal{C}_\star}{Y}$ for $\mathcal{C} \leqslant \frac{\mathcal{C}_\star}{1+\Delta\eta}$ and $\min(\mathcal{C}_{\star\star}, \frac{\alpha\mathcal{C}_\star}{1+F-\frac{\Delta\eta}{2W}(F-W)-\frac{F\Delta\eta\alpha^2}{2W}-\alpha F(1-\frac{\Delta\eta}{W})})$ for $\mathcal{C} \geqslant \frac{\mathcal{C}_\star}{1+\Delta\eta}$.

As discussed in the main text, for both $\Delta\eta \geqslant 0$ and $\Delta\eta < 0$, the transition is a plateau given by $\mathcal{C} = \mathcal{C}_{\star\star}$ when L_d/L is large enough.

[1] G. I. Taylor, Proc. R. Soc. London A **38**, 41 (1932); **146**, 501 (1934).

[2] H. A. Stone, Annu. Rev. Fluid Mech. **26**, 65 (1994).

[3] F. Leal-Calderon, V. Schmitt, and J. Bibette, *Emulsion Science, Basic Principles* (Springer, New York, 2007).

[4] D. Weaire and S. Hutzler, *The Physics of Foams* (Oxford University Press, New York, 2001).

[5] D. R. Link, S. L. Anna, D. A. Weitz, and H. A. Stone, Phys. Rev. Lett. **92**, 054503 (2004).

[6] M. De Menech, Phys. Rev. E **73**, 031505 (2006).

[7] A. M. Leshansky and L. M. Pismen, Phys. Fluids **21**, 023303 (2009).

[8] M.-C. Jullien, M.-J. Tsang Mui Ching, C. Cohen, L. Menetrier, and P. Tabeling, Phys. Fluids **21**, 072001 (2009).

[9] L. Ménétrier-Deremble and P. Tabeling, Phys. Rev. E **74**, 035303(R) (2006).

[10] A. Vananroye, P. Van Puyvelde, and P. Moldenaers, Langmuir **22**, 3972 (2006).

[11] T. Cubaud, Phys. Rev. E **80**, 026307 (2009).

[12] S. Protière, M. Z. Bazant, D. A. Weitz, and H. A. Stone, EPL **92**, 54002 (2010).

[13] M. Joanicot and A. Ajdari, Science **309**, 887 (2005).

[14] S. L. Anna, N. Bontoux, and H. A. Stone, Appl. Phys. Lett. **82**, 364 (2003).

[15] M. Belloul, W. Engl, A. Colin, P. Panizza, and A. Ajdari, Phys. Rev. Lett. **102**, 194502 (2009).

[16] J. C. McDonald, D. C. Duffy, J. R. Anderson, D. T. Chiu, H. Wu, O. J. A. Schueller, and G. M. Whitesides, Electrophoresis **21**, 27 (2000).

[17] See Supplemental Material at http://link.aps.org/supplemental/10.1103/PhysRevE.86.036317 for four high-speed movies and movie captions.

[18] D. A. Sessoms, M. Belloul, W. Engl, M. Roche, L. Courbin, and P. Panizza, Phys. Rev. E **80**, 016317 (2009).

[19] The effective viscosity $\eta_d^{eff}(h, w, \eta_d, \eta_c)$ accounts for additional viscous dissipation inside the slug, in the thin films of continuous phase between the slug and the channel walls, floor, and ceiling, and in the corners of the rectangular geometry. Considering different effective viscosities for the two gaps has a very weak effect on the results; in our model η_d^{eff} is the same in both gaps.

[20] H. Bruus, *Theoretical Microfluidics* (Oxford University Press, New York, 2008).

[21] V. Labrot, M. Schindler, P. Guillot, A. Colin, and M. Joanicot, Biomicrofluidics **3**, 012804 (2009).

[22] S. A. Vanapalli, A. G. Banpurkar, D. van den Ende, M. H. G. Duits, and F. Mugele, Lab. Chip **9**, 982 (2009).

[23] P. G. Saffman and G. I. Taylor, Proc. R. Soc. London A **245**, 312 (1958).

[24] Such a similarity is also discussed in the case of droplet breakup past a circular obstacle in [12].

[25] L. Salkin, A. Schmit, L. Courbin, and P. Panizza (unpublished).

[26] P. Panizza, W. Engl, C. Hany, and R. Backov, Colloids Surf., A **102**, 24 (2008).